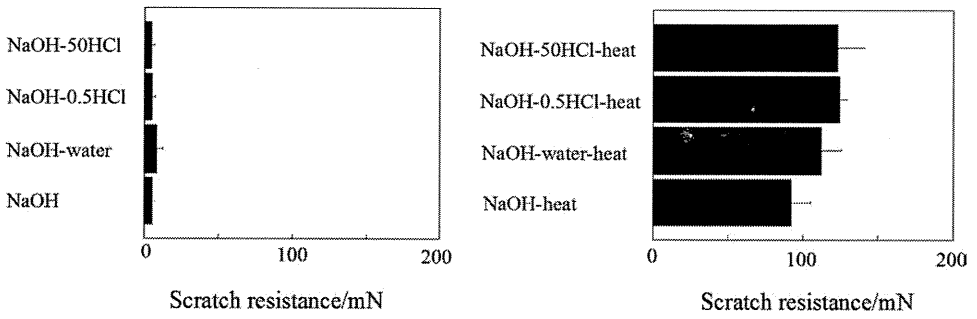

FIGURE 5. Scratch resistance of NaOH-treated Ti-15Zr-4Nb-4Ta alloy subsequently subjected to water, 0.5 HCl, or 50 HCl, and heat treatments.

the same alloy heat treated after a water and 0.5 HCl or 50 HCl treatment following the NaOH treatment showed a positive zeta potential, around +3 mV.

Apatite-forming ability in an SBF

Figure 7 shows FE-SEM photographs of the surface of alloy samples that were soaked in an SBF for 3 d after an NaOH, and water and 0.5 HCl or 50 HCl treatment, and then a heat treatment. Spherical precipitates, identified as crystalline apatite from the TF-XRD data, had formed on the surface of the NaOH-treated sample. However, these apatite particles disappeared after the subsequent heat treatment. The NaOH-treated samples subjected to a water and 0.5 HCl or 50 HCl treatment did not show the formation of apatite on their surface. However, they formed apatite extensively on their surface when they were subsequently heat treated.

Figure 8 shows the Ca 2s and P 2p XPS profiles measured from the surfaces of alloy samples soaked in an SBF after an NaOH and heat or NaOH and 50 HCl and a heat treatment as a function of the soaking time in the SBF. As can be seen from Figure 8, the alloy samples heat treated after the NaOH treatment had initially adsorbed calcium ions selectively on their surface, and then phosphate ions, whereas those samples that were heat treated after the 50 HCl treatment following an NaOH treatment had initially adsorbed phosphate ions selectively on their surface, followed by calcium ions.

DISCUSSION

It can be seen from Figure 1 that a nanometer scale roughness was produced on the surface of Ti-15-4-4 alloy by the NaOH treatment, and that this remained, even after subsequent HCl and heat treatments, as in the case of pure Ti metal.[20] The nanometer scale roughness had a brush-like structure consisting of feather-like phases elongated perpendicular to the surface to a thickness of about 500 nm (see Fig. 2). The feather-like phases consisted of nano-sized sodium hydrogen titanate ($Na_xH_{2-x}Ti_3O_7$) after the NaOH treatment. The sodium hydrogen titanate was transformed into sodium titanate ($Na_2Ti_6O_{13}$) and anatase when the alloy was immediately subjected to a heat treatment (see Figs. 3 and 4), whereas the sodium hydrogen titanate was transformed into hydrogen titanate ($H_2Ti_3O_7$) when it was soaked in water and 0.5 HCl or 50 HCl solution, and then transformed into anatase accompanied by a small amount of rutile after a subsequent heat treatment (see Figs. 3 and 4), as shown schematically in Figure 9.

The scratch resistance of the surface layer increased markedly after the heat treatment in both cases. However, the apatite-forming ability in an SBF of the alloy decreased after the heat treatment in the former case, whereas it increased markedly in the latter case. In the case of Ti metal, an apatite-forming ability of an NaOH-treated metal is increased after a subsequent heat treatment.[20] The results of the Ti-15-4-4 alloy are in contrast with those of Ti metal. These differences can be interpreted as follows. The Ti-15-4-4 alloy forms sodium titanate on its surface after the NaOH and heat treatments, as in the case of Ti metal. This sodium titanate is speculated to release sodium ions into the SBF via exchange with the oxonium ions present to form Ti-OH groups on its surface.[21,22] The Ti-OH groups formed may be negatively charged because the pH of the surrounding SBF is increased from the sodium ions released.[23] The Ti-OH groups would tend to combine with the positively charged calcium ions, and then with the phosphate ions to form apatite, as is the case for NaOH- and heat-treated Ti metal.[21,22] It was confirmed from the zeta potential data shown in Figure 6 that the Ti-15-4-4 alloy has a negatively charged surface in an NaCl solution. The sequential adsorption of the calcium and phosphate ions on the Ti-15-4-4 alloy in an SBF was confirmed by the XPS spectra shown in Figure 8.

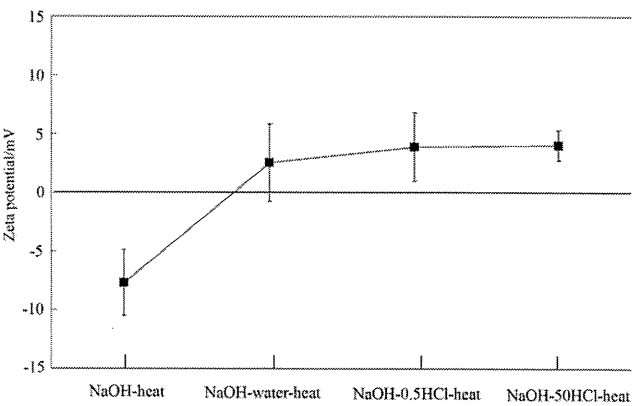

FIGURE 6. Zeta potential of NaOH-treated Ti-15Zr-4Nb-4Ta alloy subsequently subjected to water, 0.5 HCl, or 50 HCl, and heat treatments.

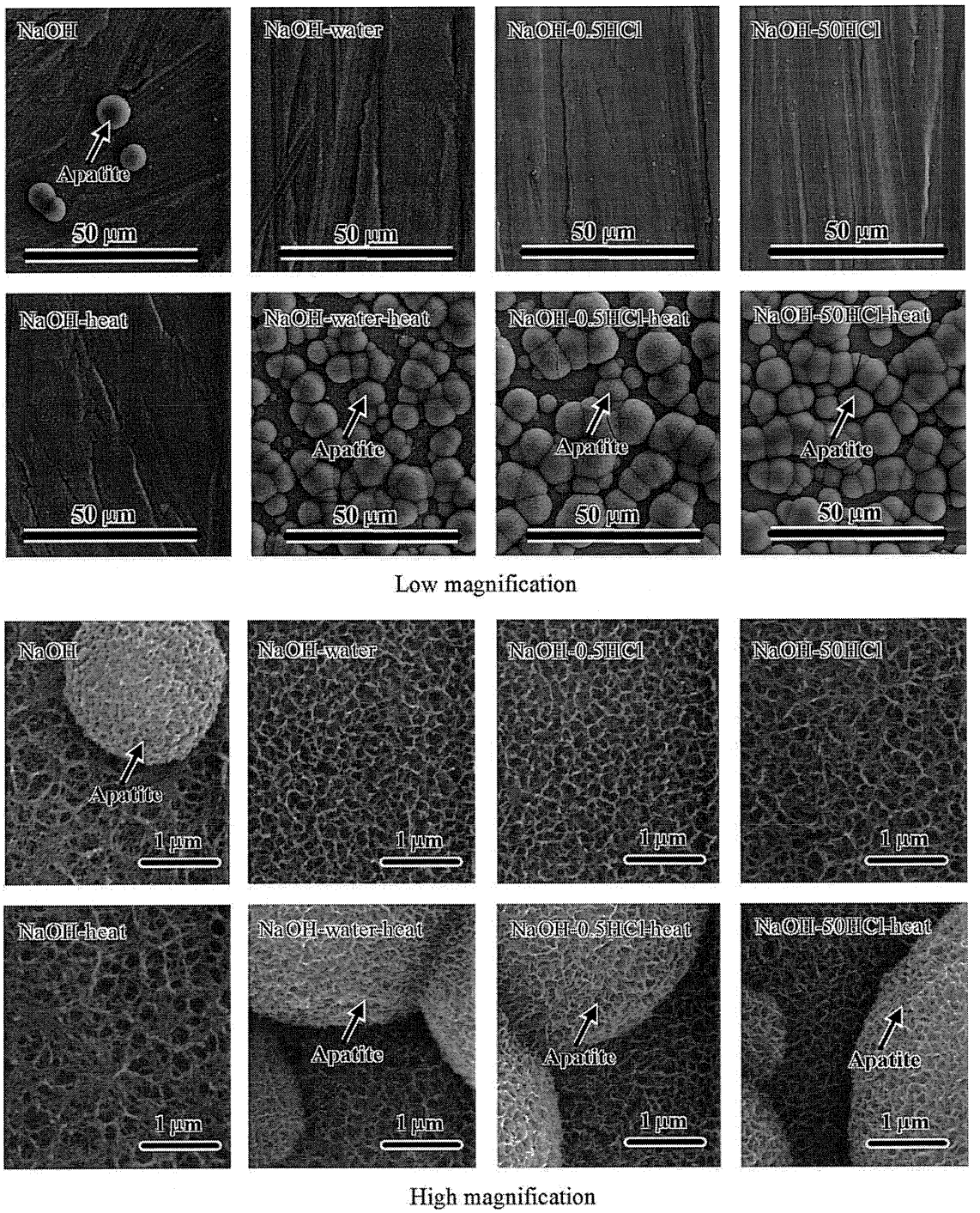

FIGURE 7. FE-SEM photographs of the surfaces of Ti-15Zr-4Nb-4Ta alloy that were soaked in SBF for 3 d after NaOH and water, 0.5 HCl, or 50 HCl, and heat treatments.

However, the thickness of the surface layer that was mainly composed of sodium titanate on the Ti-15-4-4 alloy was half that formed on Ti metal.[18] This means that the amount of sodium ions able to be released from the Ti-15-4-4 alloy was lower than that from Ti metal. In addition, the surface layer of the Ti-15-4-4 alloy contained a considerable amount of alloying elements, such as Zr, Nb, and Ta. These alloying elements can inhibit the release of sodium ions from the Ti-15-4-4 alloy. It was confirmed by measuring the release of sodium ions from the Ti-15-4-4 alloy into water that the amount and rate of sodium-ion release are low. Plate samples of the Ti-15-4-4 alloy and pure Ti metal with dimensions of $10 \times 10 \times 1$ mm^3, which were subjected to NaOH and heat treatments were soaked in 2 mL of

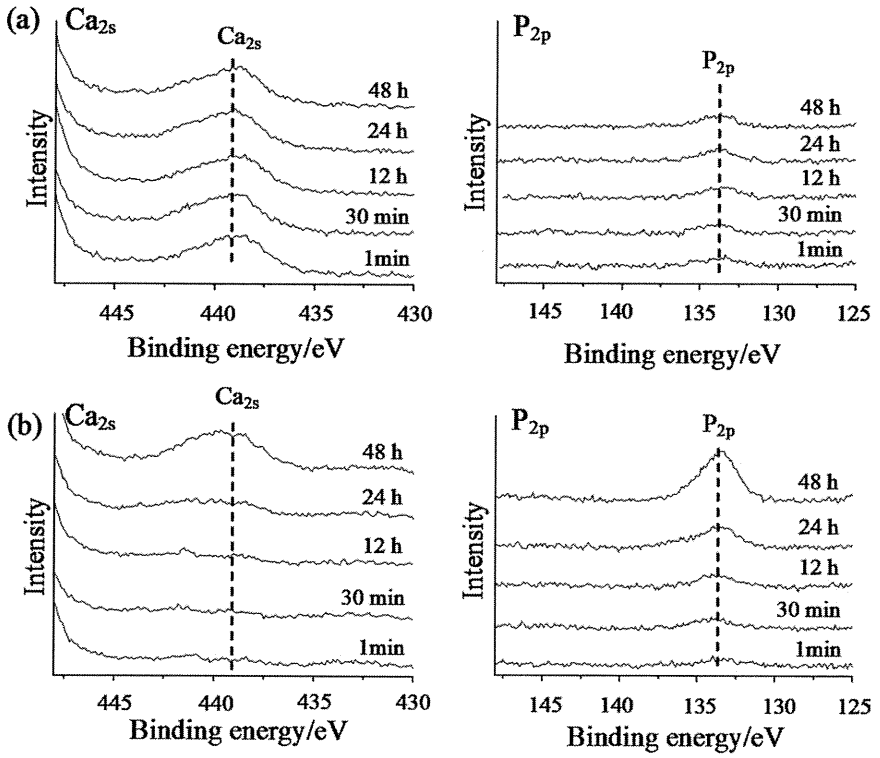

FIGURE 8. XPS profiles of the surfaces of Ti-15Zr-4Nb-4Ta alloy soaked in SBF after (a) NaOH and heat, or (b) NaOH, 50 HCl, and heat treatments as a function of soaking time in SBF.

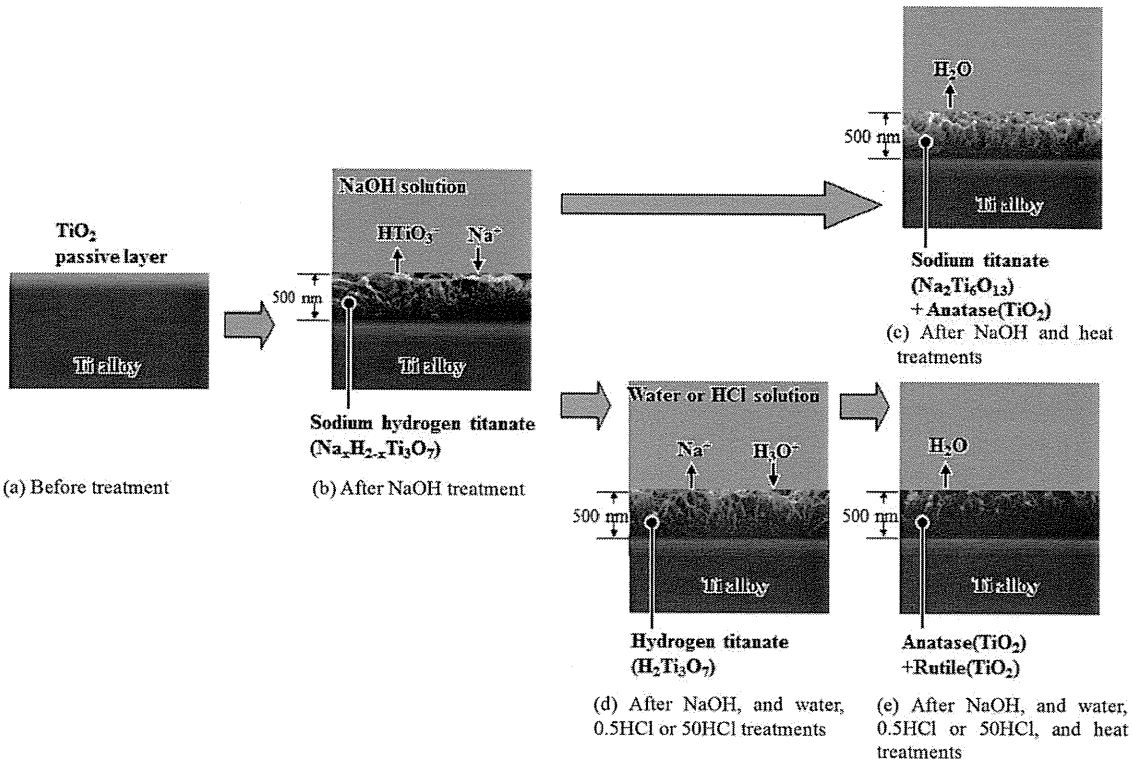

FIGURE 9. Schematic illustration of structural changes on the surface of Ti-15Zr-4Nb-4Ta alloy (a) by NaOH (b), and subsequent heat (c) treatments, or water, 0.5 HCl, or 50 HCl (d) and then heat (e) treatments.

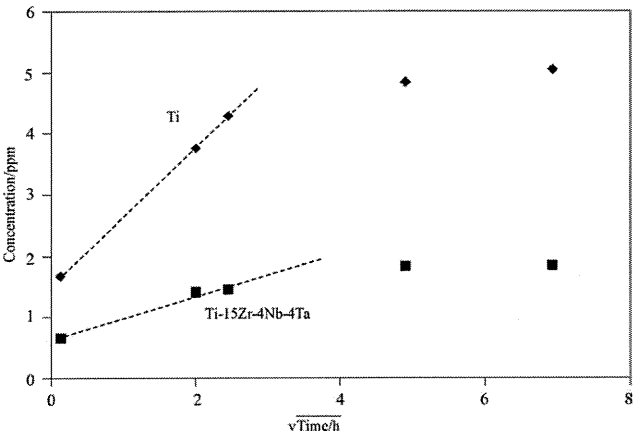

FIGURE 10. Release of sodium ions from Ti-15Zr-4Nb-4Ta alloy and Ti metal subjected to NaOH and heat treatments as a function of square root of soaking time in water, measured by ICP.

ultrapure water at 36.5°C, and the concentration of sodium ions released was measured using inductively coupled plasma (ICP, Model SPS3100, Seiko Instruments Inc., Japan) as a function of soaking time. The results shown in Figure 10 were obtained, and it can be seen that the amount and rate of release of the sodium ions from the Ti-15-4-4 alloy were markedly lower than those from pure Ti metal.

In contrast with the case of a heat treatment immediately after the NaOH treatment, the Ti-15-4-4 alloy showed a high apatite-forming ability in an SBF when it was heat treated after a water or HCl treatment following the NaOH treatment. The high apatite-forming ability of the Ti-15-4-4 alloys subjected to a water or HCl and heat treatment after the NaOH treatment can be interpreted in terms of the surface charge. As show in Figure 6, the surfaces of the Ti-15-4-4 alloy have positive charge after the water or HCl and heat treatments following the NaOH treatment. When the alloy has a positive charge on its surface, it combines selectively with negatively charged phosphate ions. As the phosphate ions begin to accumulate, its surface becomes negatively charged and combines with the positively charged calcium ions to form apatite. Such a sequential adsorption was confirmed by the XPS spectra shown in Figure 8.

The positive surface charge of the alloys subjected to HCl and heat treatments after the NaOH treatment may be attributed to the presence of chloride ions adsorbed on the surface, as in the case of Ti metal.[11] These chloride ions are adsorbed on the surface of the alloy during the HCl treatment after the NaOH treatment. These remain after the subsequent heat treatment and dissociate in the SBF to give an acidic environment on the surface of the alloy.[11] Titanium oxide is positively charged in an acid environment.[23]

In the case of Ti metal, the positive surface charge and the apatite-forming ability are increased with increasing concentration of the HCl solution,[13] because a higher concentration of chloride ions can be adsorbed on the surface in a concentrated HCl solution. However, the alloy treated with 50 HCl solution showed almost the same zeta potential and apatite-forming ability as the sample treated with the 0.5 HCl solution (see Figs. 6 and 7). This is interpreted in terms of the increased amount of alloying elements, such as Zr and Nb, after the 50HCl treatment (see Table I). It has been reported that the typical isoelectric points (IEPs) of ZrO_2 and Nb_2O_5 are around 6.5[24] and 4.1.[25] This means that both zirconium oxide and niobium oxide tend to be negatively charged at pH =7.4 in an SBF, and hence, the increase in Zr and Nb content can decrease the surface charge of the Ti-15-4-4 alloy subjected to a 50 HCl treatment.

On the other hand, the positive surface charge of the alloy subjected to water and heat treatments after the NaOH treatment cannot be interpreted in terms of the presence of chloride ions adsorbed on the alloy. It has been reported that anatase is the main phase on the surface layer of Ti-15-4-4 alloys subjected to a water and heat treatment after an NaOH treatment, and that this is slightly negatively charged in a neutral aqueous solution because its IEP value is around 6.[26] However, this value changes to within the range 4.0 to 8.3 in the presence of a small amount of impurities, or changes in the synthesis method.[27] As shown in Table I, the surface layer formed on the alloy after a water and heat treatment following the NaOH treatment contained some Zr, Nb, and Ta besides Ti and O. These elements can be incorporated into the anatase and give a positive surface charge in an SBF. It has also been reported that the surface charge of the anatase changes with crystallographic plane orientation. The (101) plane has a negative surface charge,[28] while the (001) plane has a positive surface charge.[29] Therefore, the positive surface charge on the alloy subjected to a water and heat treatment after the NaOH treatment may be interpreted in terms of the presence of impurities and/or preferred orientation of a specific crystallographic plane of the anatase.

It is apparent from our results and discussion that water or HCl and a heat treatment after the NaOH treatment forms a titanium oxide surface layer that has a nanometer scale roughness and a high apatite-forming ability on a Ti-15-4-4 alloy. Their high apatite-forming ability is attributed to their positive surface charge. Such treated porous Ti-15-4-4 alloys are expected to exhibit osteoconductivity as well as osteoinductivity, and hence, will be useful in implants in the orthopedic and dental fields. These biological properties will be examined by animal experiments in future.

CONCLUSIONS

Water or HCl and heat treatments were applied to Ti-15Zr-4Nb-4Ta alloys after an NaOH treatment. A nanometer scale roughness was produced on the surface of the alloys by the NaOH treatment, and this remained, even after a subsequent water or HCl and heat treatment. These treatments formed a titanium oxide layer that was mainly composed of anatase on the surface of the alloys. This showed a high apatite-forming ability in an SBF, as well as a high scratch resistance. The high apatite-forming ability was interpreted in terms of the positive surface charge. In contrast with this, Ti-15Zr-4Nb-4Ta alloys subjected to a heat treatment without a water or HCl treatment after the NaOH treatment did

not form apatite in an SBF. This was attributed to slow rate of release of the sodium ions from the alloy in the SBF. It is expected that such treated Ti-15Zr-4Nb-4Ta alloys subjected to a water or HCl treatment after an NaOH treatment will form an apatite layer on their surface in a living body, and will tightly bond to living bone through this apatite layer. Therefore, they will be useful as orthopedic and dental implants.

ACKNOWLEDGMENTS

The authors thank Dr. Yoshimitsu Okazaki for the supply of the alloy.

REFERENCES

1. Kokubo T, Miyaji F, Kim HM, Nakamura T. Spontaneous formation of bone-like apatite layer on chemically treated titanium metal. J Am Ceram Soc 1996;79:1127–1129.
2. Kokubo T, Miyaji F, Kim HM, Nakamura T. Preparation of bioactive Ti and its alloy via simple chemical surface treatment. J Biomed Mater Res 1996;32:409–417.
3. Yan QW, Nakamura T, Kobayashi M, Kim HM, Kokubo T. Bonding of chemically treated titanium implants to bone. J Biomed Mater Res 1997;37:267–275.
4. Nishiguchi S, Fujibayashi S, Kim HM, Kokubo T, Nakamura T. Biology of alkali- and heat- treated titanium implants. J Biomed Mater Res A 2003;67:26–35.
5. Kawanabe K, Ise K, Goto K, Akiyama H, Nakamura T, Kaneuji A, Sugimori T, Mtsumoto T. Clinical device-related article a new cementless total hip arthroplasty with bioactive titanium porous-coating by alkaline and heat treatment: Average 4.8-year results. J Biomed Mater Res B Appl Biomater 2009;90:476–481.
6. Kim HM, Takadama H, Miyaji F, Kokubo T, Nishiguchi S, Nakamura T. Formation of bioactive functionally graded structure on Ti-6Al-4V alloy by chemical surface treatment. J Mater Sci Mater Med 2000;11:555–559.
7. Kim HM, Takadama H, Kokubo T, Nishiguchi S, Nakamura T. Formation of a bioactive graded surface structure on Ti-15Mo-5Zr-3Al alloy by chemical treatment. Biomaterials 2000;21:353–358.
8. Geetha M, Singh AK, Asokamani R, Gogia AK. Ti based biomaterials, the ultimate choice for orthopedic implants—A review. Prog Mater Sci 2009;54:397–425.
9. Okazaki Y, Rao S, Ito Y, Tateishi T. Corrosion resistance, mechanical properties, corrosion fatigue strength and cytocompatibility of new Ti alloys without Al and V. Biomaterials 1998;19:1197–1215.
10. Yamaguchi S, Takadama H, Matsushita T, Nakamura T, Kokubo T. Apatite-forming ability of Ti-15Zr-4Nb-4Ta alloy induced by calcium solution treatment. J Mater Sci Mater Med 2010;21:439–444.
11. Kokubo T, Pattanayak DK, Yamaguchi S, Takadama H, Matsushita M, Kawai T, Takemoto M, Fujibayashi S, Nakamura T. Positively charged bioactive Ti metal prepared by simple chemical and heat treatments. J R Soc Interface 2010;7:S503–S513.
12. de Brujin JD, Shankar K, Yuan H, Habibovic P. Osteoinduction and its evaluation. In: Kokubo T, editor, Bioceramics and their Clinical Applications. Cambridge: Woodhead; 2008. p 199–219.
13. Pattanayak DK, Kawai T, Matsushita T, Takadama H, Nakamura T, Kokubo T. Effect of HCl concentrations on apatite-forming ability of NaOH-HCl-heat-treated titanium metal. J Mater Sci Mater Med 2009;20:2401–2411.
14. Fujibayashi S, Nakamura T, Nishiguchi S, Tamura J, Uchida M, Kim HM, Kokubo T. Bioactive titanium: Effect of sodium removal on the bone-bonding ability of bioactive titanium prepared by alkali and heat treatment. J Biomed Mater Res 2001;56: 562–570.
15. Takemoto M, Fujibayashi S, Neo M, Suzuki J, Matsushita T, Kokubo T, Nakamura T. Osteoinductive porous titanium implants: Effect of sodium removal by dilute HCl treatment, Biomaterials 2006;27:2682–2691.
16. Sugino A, Ohtsuki C, Tsuru K, Hayakawa S, Nakano T, Okazaki Y, Osaka A. Effect of spatial design and thermal oxidation on apatite formation on Ti-15Zr-4Ta-4Nb alloy, Acta Biomater 2009;5: 298–304.
17. Kokubo T, Takadama H. How useful is SBF in predicting in vivo bone bioactivity? Biomaterials 2006;27:2907–2915.
18. Yamaguchi S, Takadama T, Matsushita T, Nakamura T, Kokubo T. Cross-sectional analysis of the surface ceramic layer developed on Ti metal by NaOH-heat treatment and soaking in SBF. J Ceram Soc Japan 2009;117:1126–1130.
19. Sun X, Li Y. Synthesis and characterization of ion-exchangeable titanate nanotubes. Chem Eur J 2003;9:2229–2238.
20. Kawai T, Kizuki T, Takadama H, Matsushita T, Kokubo T, Unuma H, Nakamura T. Apatite formation on surface titanate layer with different Na content on Ti metal. J Ceram Soc Japan 2010;9:19–24.
21. Kim HM, Himeno T, Kawashita M, Lee JH, Kokubo T, Nakamura T. Surface potential change in bioactive titanium metal during the process of apatite formation in simulated body fluid. J Biomed Mater Res A 2003;67:1305–1309.
22. Takadama H, Kim HM, Kokubo T, Nakamura T. TEM-EDX Study of mechanism of bonelike apatite formation on bioactive titanium metal in simulated body fluid. J Biomed Mater Res 2001;57:441–448.
23. Textor M, Sitting C, Franchiger V, Tosatti S, Brunette DM. Properties and biological significance of natural oxide films on titanium and its alloys. In: Brunette DM, Tengrall P, Textor M, Thomsen P, editors. Tianium in Medicine. Verlag: Springer; 2001. p172–230.
24. Hook MS, Hartley PG, Thistlethwaite PJ. Fabrication and characterization of spherical zirconia particles for direct force measurement using the atomic force microscope. Langmuir 1999;15: 6220–6225.
25. Kosmulski M. Attempt to determine pristine points of zero charge of Nb_2O_5, Ta_2O_5, and HfO_2. Langmuir 1997;13:6315–6320.
26. Kiyono M. Sanka titan-bussei to ouyougijutsu. Japan: Gihodo; 1991.
27. Kosmulski M. Surface Charging and Points of Zero Charge. US: CRC press; 2009.
28. Barnard AS, Zapol P, Curtiss LA. Modeling the morphology and phase stability of TiO_2 nanocrystals in water. J Chem Theory Comput 2005;1:107–116.
29. Blomquist J, Walle IF, Uvdal P, Borg A, Sandell A. Water dissociation on single crystalline anatase TiO_2(001) studied by photoelectron spectroscopy. J Phys Chem C Nanomater Interfaces 2008; 112:16616–16621.

The long-term in vivo behavior of polymethyl methacrylate bone cement in total hip arthroplasty

Hiroyuki Oonishi[1*], Haruhiko Akiyama[2*], Mitsuru Takemoto[2], Toshiyuki Kawai[2], Koji Yamamoto[2], Takao Yamamuro[3], Hironobu Oonishi[1], and Takashi Nakamura[2]

* These authors contributed equally to this work.

[1]H. Oonishi Memorial Joint Replacement Institute, Tominaga Hospital, Osaka; [2] Department of Orthopaedics, Kyoto University, Kyoto; [3]Research Institute for Production Development, Kyoto, Japan
Correspondence: hakiyama@kuhp.kyoto-u.ac.jp
Submitted 11-02-01. Accepted 11-06-28

Background and purpose The long-term success of cemented total hip arthroplasty (THA) has been well established. Improved outcomes, both radiographically and clinically, have resulted mainly from advances in stem design and improvements in operating techniques. However, there is concern about the durability of bone cement in vivo. We evaluated the physical and chemical properties of CMW1 bone cements retrieved from patients undergoing revision THA.

Methods CMW1 cements were retrieved from 14 patients who underwent acetabular revision because of aseptic loosening. The time in vivo before revision was 7–30 years. The bending properties of the retrieved bone cement were assessed using the three-point bending method. The molecular weight and chemical structure were analyzed by gel permeation chromatography and Fourier-transform infrared spectroscopy. The porosity of the bone cements was evaluated by 3-D microcomputer tomography.

Results The bending strength decreased with increasing time in vivo and depended on the density of the bone cement, which we assume to be determined by the porosity. There was no correlation between molecular weight and time in vivo. The infrared spectra were similar in the retrieved cements and in the control CMW1 cements.

Interpretation Our results indicate that polymer chain scission and significant hydrolysis do not occur in CMW1 cement after implantation in vivo, even in the long term. CMW1 cement was stable through long-term implantation and functional loading.

The concept behind Charnley low-friction arthroplasty was established in the 1960s, and the fundamental principles have remained unchanged since then. Several clinical studies have recently reported the long-term success of total hip arthroplasty (THA). Wroblewski et al. (2009) reported good results using Charnley low-friction arthroplasty with a follow-up of 30–40 years. Overall, 90% of hips were free from pain, and activity was normal in 59% of the patients. Carrington et al. (2009) reported the results of the Exeter Universal cemented femoral component after 15–17 years. With an endpoint of revision for aseptic loosening, the survivorship at 17 years was 100% for the femoral component and 90% for the acetabular component. With all reasons for reoperation as the endpoint, the survivorship was 81%. A variety of cemented stems designed according to various concepts have been used, and several improvements have been incorporated into the operating techniques (Madey et al. 1997, Noble et al. 1998, Scheerlinck and Casteleyn 2006). Although self-curing polymethyl methacrylate (PMMA) bone cements have been used for fixation of the implants for the past 50 years, the composition of the cements has remained essentially unaltered. The ultra-long clinical and radiographic success of cemented THA may depend on the mechanical and chemical longevity of the bone cements in vivo.

Several authors have reported on the in vivo behavior of PMMA bone cement in the implanted joint. Some studies have shown aging of PMMA in vivo. Hughes et al. (2003) showed a decrease in molecular weight and hydrolysis of PMMA associated with long-term implantation. Looney and Park (1986) reported a reduction in flexural strength but not in compressive strength. Fernandez-Fairen and Vazquez (1983) analyzed the compressive properties of the retrieved CMW1 cements and found a decrease in the compressive modulus and strength after long implantation periods. By contrast, Ries et al. (2006) concluded that the most important factor for the mechanical properties of bone cement in vivo is not the implant duration but the porosity. It remains unknown whether the mechanical and chemical properties of bone cement change in vivo, and how these changes affect the long-term outcome of cemented

DOI 10.3109/17453674.2011.625538

THA. We investigated various properties, including molecular weight, chemical structure, bending properties, density, and porosity in retrieved bone cements.

Patients and methods

Sample preparation

CMW1 cements were retrieved from 14 patients who underwent acetabular revision because of aseptic loosening. The median time in vivo before revision was 15 (7–30) years. The retrieved samples were rinsed in saline solution and ethanol, and then stored at room temperature until they were examined.

Molecular weight analysis

The average molecular weight and the molecular weight distribution of the retrieved cements were assessed by gel permeation chromatography (GPC). Molecular weight calibration was established based on polystyrene standards. Briefly, samples were dissolved in tetrahydrofuran (THF) to a concentration of 2 mg/mL at room temperature, and then filtered through 0.45-μm disk filters. Each sample was injected into a 30-cm long GPC gel column (Shodex, Tokyo, Japan) with an inner diameter of 8.0 mm, which was packed with THF with a pore size of 1,000 nm. The injection volume was 50 μL and the flow rate was 1 mL/min at 40°C. A differential refractive index detector (Hitachi L-2000; Hitachi, Tokyo, Japan) was used to monitor changes in the concentration of the sample. The molecular weight distributions of the samples relative to polystyrene were found in terms of the number-averaged molecular weight M_n, the weight-averaged molecular weight M_w, and the polydispersity index (PDI; M_w/M_n ratio).

Fourier-transform infrared spectroscopy (FTIR) analysis

Chemical analysis was performed using FTIR. The FTIR spectra were obtained using a Spectrum BX spectrometer (PerkinElmer, Waltham, MA). All transmission spectra were collected with a spectral resolution of 4 cm^{-1} and spectral range of 4000 to 600 cm^{-1} using KBr pellets. Unimplanted control CMW1 cement specimens were freshly prepared by mixing the powder and liquid components by hand according to the manufacturer's instructions. They were then sent for FTIR analysis within 1 month of preparation.

Bending properties

The retrieved cement specimens were cut and scraped into rectangular specimens (20 mm × 4 mm × 3 mm) using a rotational scraping machine (BUEHLER EcoMet 3000; BUEHLER Ltd., Lake Bluff, IL) with 1–9 specimens for each sample. The bending strength and bending modulus of each retrieved cement specimen and each freshly prepared CMW1 cement specimen were analyzed using an Instron 5500 instrument (Instron, Norwood, MA) at 23 ± 1°C. The crosshead speed and the span were 0.5 mm/min and 15 mm, respectively, when using the 3-point bending method. The values for the bending modulus were derived from the stress-strain curves obtained from the bending tests, as described previously (Shinzato et al. 2002).

Summary of molecular weights for the retrieved cements

Sample no.	Implantation time (years)	M_w (g/mol)	M_n (g/mol)	PDI
1	7	209,737	66,412	3.16
2	7	199,478	68,608	2.91
3	7	220,660	74,217	2.97
4	10	187,296	67,205	2.79
5	10	208,271	64,416	3.23
6	10	217,552	71,617	3.04
7	13	176,996	63,839	2.77
8	13	196,600	67,618	2.91
9	14	192,056	70,209	2.74
10	16	211,157	66,509	3.17
11	21	216,827	62,554	3.47
12	25	203,630	62,005	3.28
13	26	192,270	61,753	3.11
14	30	212,962	66,750	3.19

Porosity analysis

A microfocus X-ray computed tomography system (SMX-100CT-SV3; Shimadzu Co., Kyoto, Japan) was used to acquire microstructural information from the retrieved cements. The entire set of radiographs was deconvoluted by computer software to reconstruct a 3-D image of the microstructure with a voxel size of 16 μm^3. The 3-D data were processed with commercially available 3-D image-processing software (VG Studio MAX 2.0; Volume Graphics, Heidelberg, Germany), and the porosity of the retrieved cements was calculated from the binary material images. The spatial boundary between the pores and the cement was established easily because of the large differences in density.

Statistics

Data from each test were compared by analysis of variance (ANOVA) to determine the overall significance of data trends. For all analyses, $p < 0.01$ was considered significant.

Results

The M_w of the samples ranged from 170,000 to 220,000 g/mol (Table). The molecular weight and PDI did not correlate with the time in vivo ($r = 0.013$, $p = 1.0$; $r = 0.54$, $p = 0.05$, respectively) (Figure 1A and B). Because the molecular weight of the polymer is proportional to the degree of polymerization of the monomer unit, this result suggested that scission of polymer chains did not occur in CMW1

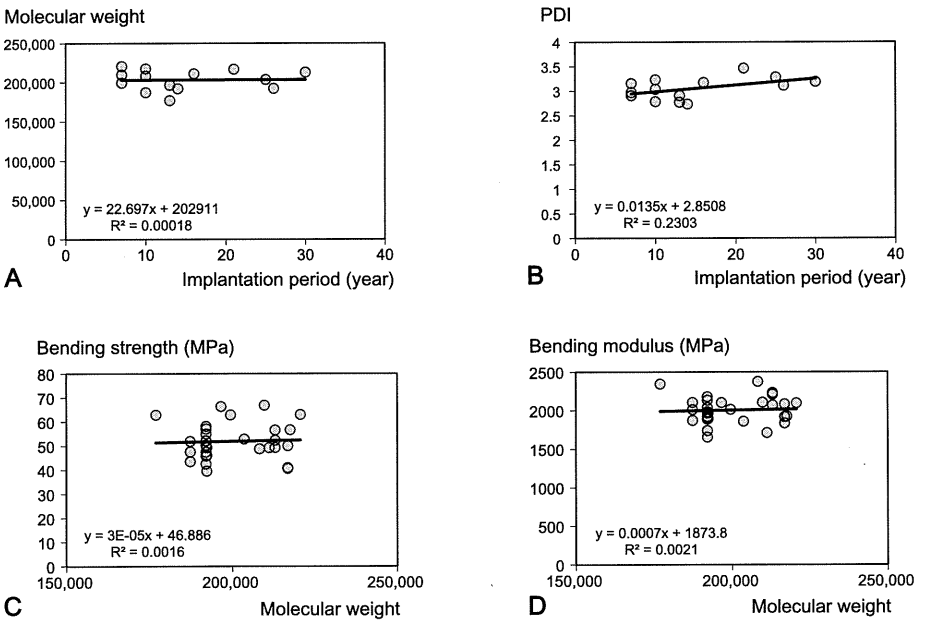

Figure 1 A. Relationship between implantation period and molecular weight. B. Relationship between implantation period and PDI. C. Relationship between molecular weight and bending strength. D. Relationship between molecular weight and bending modulus.

cement in vivo. There was no substantial difference in FTIR spectra between the CMW1 cements in fresh samples after they were cured and in samples retrieved 16 and 30 years after implantation (Figure 2). The spectra of methyl methacrylate homopolymer showed a distinctive absorbance band around 1,730 cm^{-1}, corresponding to the C=O stretch of the ester group (Hughes et al. 2003). This distinctive absorbance band did not differ between freshly prepared and retrieved CMW1 cements. These results indicate that no substantial hydrolysis of the ester group occurred in CMW1 cement in vivo, even after many years.

The molecular weight was not related to the bending strength or the bending modulus (r = 0.040, p = 0.83; r = 0.046, p = 0.8, respectively) (Figure 1C and D). By contrast, the bending strength of each cement specimen was reduced with increasing time in vivo, but this was not statistically significant (r = –0.39, p = 0.03) (Figure 3A). In addition, there was no correlation between bending modulus and the length of the implantation period (r = –0.038, p = 0.8) (Figure 3B).

The density of the specimens was calculated from their dimension and weight. There was no correlation between the density of the cements and length of time in vivo (r = –0.20, p = 0.3) (Figure 4A). Density was found to be strongly correlated to bending strength (r = 0.54, p = 0.002) but not to bending modulus (r = 0.38, p = 0.04) (Figure 4B and C). There was no correlation between the porosity of the specimens and the time in vivo (r = 0.27, p = 0.1) (Figure 5A). There was a strong correlation between the density and the porosity of

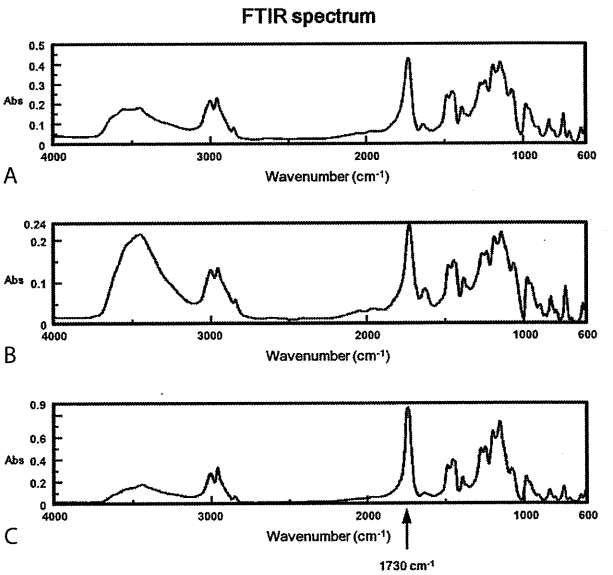

Figure 2. FTIR spectrum of control CMW1 cement (A) and CMW1 cement retrieved 16 years (B) and 30 years (C) after implantation.

the cement (r = –0.67, p < 0.001) (Figure 5B). The porosity correlated with bending strength (r = –0.51, p = 0.004) (Figure 5C) but not with bending modulus (r = –0.18, p = 0.4) (Figure 5D). These results indicate that the porosity of the

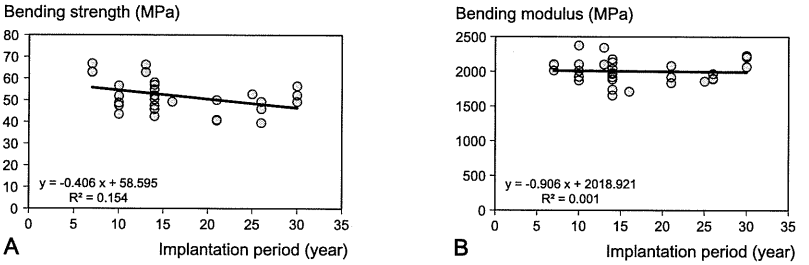

Figure 3. A. Relationship between implantation period and bending strength. B. Relationship between implantation period and bending modulus.

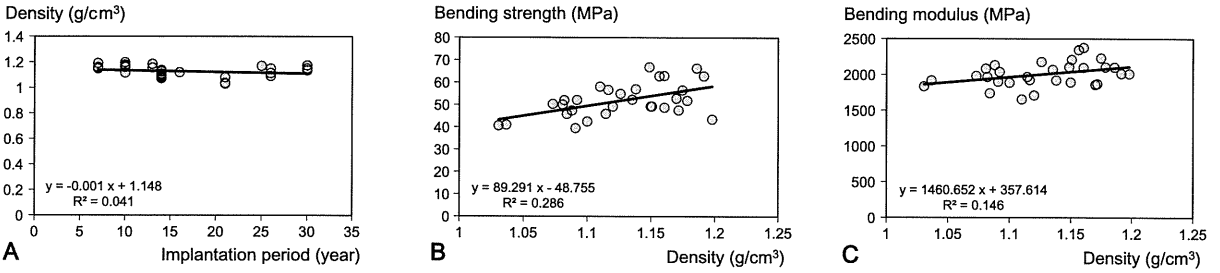

Figure 4. A. Relationship between implantation period and density. B. Relationship between density and bending strength. C. Relationship between density and bending modulus.

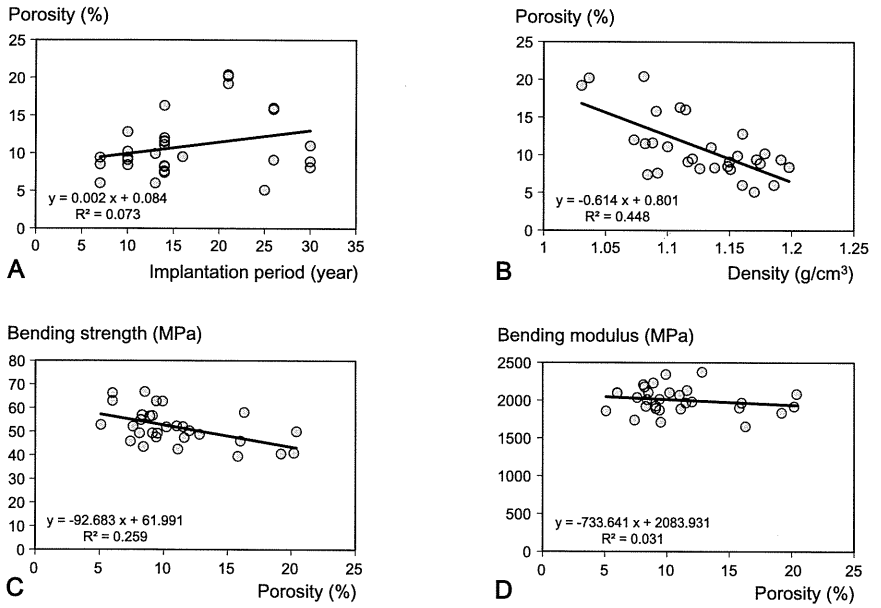

Figure 5. A. Relationship between implantation period and porosity. B. Relationship between density and porosity. C. Relationship between porosity and bending strength. D. Relationship between porosity and bending modulus.

bone cement defined the in vivo mechanical properties of the retrieved specimens. As the porosity of cement is unlikely to change substantially after curing, the mechanical properties of the cement should remain stable.

Discussion

One of the factors that dictate the long-term stability of cemented stems is the longevity of the cement itself. Failure of the cemented stem implanted in THAs is induced by excessive stress in the cement mantle, leading to micromovement of the stem and debonding at the cement-stem interface, along with microcracking in the cement (Gardiner and Hozack 1994, Ong et al. 2002). This cement damage finally causes stem loosening, stem subsidence, increased production of wear particles, and osteolysis. Thus, retention of the chemical and mechanical properties of the bone cement in vivo is critical for achievment of long-term success in THA.

Although previous studies have used various tests to investigate the in vivo behavior and chemical and mechanical properties of bone cements, there is no consensus on the aging of the cement (Fernandez-Fairen and Vazquez 1983, Looney and Park 1986, Hughes et al. 2003, Ries et al. 2006). The molecular structure, the dispersity of the contrast medium, or the distribution of pores introduced during the preparation of bone cements may affect their mechanical properties, and these complex factors make interpretation of the data—and comparison between studies—difficult.

The mechanical properties of implanted bone cements depend on the chemistry of the bone cement and on the mixing method (Lewis 1997). Our study shows that there is no correlation between the molecular weight of the bone cement and the time in vivo, and that neither degradation of the main chain nor hydrolysis of PMMA occurs in CMW1 cement. We also found no relationship between molecular weight and bending strength or bending modulus. Our results contrast with those of Hughes et al. (2003), who found a decrease in molecular weight and chemical degradation in retrieved Simplex P and Palacos R cements that had aged up to 23 years in vivo. CMW1 powder comprises only methyl methacrylate, whereas Palacos R powder contains methylacrylate, which is polar and hydrophilic. Simplex P contains hydrophobic styrene comonomer, which has no polarity. In vivo degradation of bone cements is related to particular combinations of localized acidic pH, free radical oxidation induced by superoxidizing substances, and hydrolyzing enzymes. One possible explanation of these results (Hughes et al. 2003) that the differences in chemical properties of bone cements confer different sensitivities to biological processes that induce degradation. The cements retrieved from total knee arthroplasties after similar in vivo aging times to those from THAs showed little change in their structural properties, suggesting that in vivo degradation of the bone cements is related to the biological response to the implant and the local environment of the joint (Hughes et al. 2003). These lines of evidence strongly suggest that the degradation of bone cements in vivo depends partly on the environment of implantation and partly on the composition of bone cements. In addition, the FTIR spectra showed an increase in the large band at 3,500 cm-1, attributable to OH stretching in water, in some retrieved specimens. Water is a plasticizer for methacrylate, and could therefore reduce the mechanical properties of bone cement. This should be clarified by further studies.

Although Dall et al. (2007) reported that inter-batch and intra-batch variability was seen in the viscosity of all brands of bone cement, the strong relationship between bending strength and density or porosity shows that the mechanical properties of bone cements depend on their density or porosity (Weinstein et al. 1976, Wang et al. 1993, Chaplin et al. 2006). Our study and studies of others have shown significant correlations between density and porosity. High porosity contributes to microcracks in the bone cement, which lead to release of PMMA particles and induce aseptic loosening and osteolysis (James et al. 1992, Graham et al. 2003, Hoey et al. 2009). In addition, cracks and voids could be also generated by micromovement between cement and prosthesis/bone or by wear, and may affect the mechanical properties. Thus, the porosity of bone cement is a critical factor in determining the mechanical properties of the bone cement in vivo. The porosity of bone cement is determined by the method used to prepare and apply it. In the modern cementing technique, vacuum mixing reduces the porosity of bone cement and improves its fatigue resistance (James et al. 1992, Wang et al. 1993). Graham et al. (2000) reported that the internal porosity of bone cement is greatly reduced by vacuum mixing, whereas a higher porosity introduced during the hand-mixing process caused all hand-mixed specimens to have inferior fracture and fatigue resistance to their vacuum-mixing counterparts. Moreover, elevated pressure during curing helps reduce the porosity of the bone cement; thus, high-pressure insertion of implants substantially improves the mechanical properties of the bone cement (Bayne et al. 1975, Apostolou et al. 2007). Taken together, this evidence shows that the mechanical properties of implanted bone cement depend on the operating techniques rather than the period of implantation.

Ries et al. (2006) investigated the variables fracture toughness, porosity, molecular weight, and time in vivo of the bone cement, and concluded that porosity and fracture toughness are significantly and inversely related. All bone cements retrieved in the acetabular reconstruction in our study were hand-mixed and were applied to the acetabulum without use of a cement pressurizer. One possible reason that the porosity increases in relation to the time in vivo is that cement pressurization in the implantation of the acetabular component has been improved by the development of operation instruments, including the component holder and component pusher, which reduce the initial porosity of the bone cement. These lines of evidence also suggest that the mechanical properties of bone cement in vivo are strongly affected by the cementing techniques.

In conclusion, we found that the properties of bone cement were determined by the porosity of the cement but were not affected by the length of the period of implantation. The chemical structure of CMW1 cement was stable in vivo even after more than 20 years.

HO performed the experiments and participated in writing of the manuscript. HA coordinated the study, participated in design of the protocol, performed the experiments, analyzed the data, and participated in writing of the manuscript. MT analyzed the data and participated in writing of the manuscript. TK performed the experiments and analyzed the data. KY analyzed the data. TY participated in design of the protocol. HO participated in design of the protocol and prepared the samples. TN obtained funding and participated in design of the protocol.

No competing interests declared.

Apostolou C D, Yiannakopoulos C K, Ioannidis T T, Papagelopoulos P J, Korres D. Mechanical stability of total hip replacement using pressurization of bone cement during curing: push-out tests in cadaver femora. Orthopedics 2007; 30 (12): 1028-32.

Bayne S C, Lautenschlager E P, Compere C L, Wildes R. Degree of polymerization of acrylic bone cement. J Biomed Mater Res 1975; 9 (1): 27-34.

Carrington N C, Sierra R J, Gie G A, Hubble M J, Timperley A J, Howell J R. The Exeter Universal cemented femoral component at 15 to 17 years: an update on the first 325 hips. J Bone Joint Surg (Br) 2009; 91 (6): 730-7.

Chaplin R P, Lee A J, Hooper R M, Clarke M. The mechanical properties of recovered PMMA bone cement: a preliminary study. J Mater Sci Mater Med 2006; 17 (12): 1433-48

Dall G F, Simpson P M, Mackenzie S P, Breusch S J. Inter- and intra-batch variability in the handling characteristics and viscosity of commonly used antibiotic-loaded bone cements. Acta Orthop 2007; 78 (3): 412-20

Fernandez-Fairen M, Vazquez J J. The aging of polymethyl methacrylate bone cement. Acta Orthop Belg 1983; 49 (4): 512-20.

Gardiner R C, Hozack W J. Failure of the cement-bone interface. A consequence of strengthening the cement-prosthesis interface? J Bone Joint Surg (Br) 1994; 76(1): 49-52.

Graham J, Pruitt L, Ries M, Gundiah N. Fracture and fatigue properties of acrylic bone cement: the effects of mixing method, sterilization treatment, and molecular weight. J Arthroplasty 2000; 15 (8): 1028-35.

Graham J, Ries M, Pruitt L. Effect of bone porosity on the mechanical integrity of the bone-cement interface. J Bone Joint Surg (Am) 2003; 85 (10): 1901-8.

Hoey D, Taylor D. Quantitative analysis of the effect of porosity on the fatigue strength of bone cement. Acta Biomater 2009; 5 (2): 719-26

Hughes K F, Ries M D, Pruitt L A. Structural degradation of acrylic bone cements due to in vivo and simulated aging. J Biomed Mater Res A 2003; 65 (2): 126-35.

James S P, Jasty M, Davies J, Piehler H, Harris W H. A fractographic investigation of PMMA bone cement focusing on the relationship between porosity reduction and increased fatigue life. J Biomed Mater Res 1992; 26 (5): 651-62.

Lewis G. Properties of acrylic bone cement: state of the art review. J Biomed Mater Res 1997; 38 (2): 155-82.

Looney M A, Park J B. Molecular and mechanical property changes during aging of bone cement in vitro and in vivo. J Biomed Mater Res 1986; 20 (5): 555-63.

Madey S M, Callaghan J J, Olejniczak J P, Goetz D D, Johnston R C. Charnley total hip arthroplasty with use of improved techniques of cementing. The results after a minimum of fifteen years of follow-up. J Bone Joint Surg (Am) 1997; 79 (1): 53-64.

Noble P C, Collier M B, Maltry J A, Kamaric E, Tullos H S. Pressurization and centralization enhance the quality and reproducibility of cement mantles. Clin Orthop 1998; (355): 77-89.

Ong A, Wong K L, Lai M, Garino J P, Steinberg M E. Early failure of precoated femoral components in primary total hip arthroplasty. J Bone Joint Surg (Am) 2002; 84 (5): 786-92.

Ries M D, Young E, Al-Marashi L, Goldstein P, Hetherington A, Petrie T, Pruitt L. In vivo behavior of acrylic bone cement in total hip arthroplasty. Biomaterials 2006; 27 (2): 256-61.

Scheerlinck T, Casteleyn P P. The design features of cemented femoral hip implants. J Bone Joint Surg (Br) 2006; 88 (11): 1409-18.

Shinzato S, Nakamura T, Ando K, Kokubo T, Kitamura Y. Mechanical properties and osteoconductivity of new bioactive composites consisting of partially crystallized glass beads and poly(methyl methacrylate). J Biomed Mater Res 2002; 60 (4): 556-63

Wang J S, Franzen H, Jonsson E, Lidgren L. Porosity of bone cement reduced by mixing and collecting under vacuum. Acta Orthop Scand 1993; 64 (2): 143-6.

Weinstein A M, Bingham D N, Sauer B W, Lunceford E M. The effect of high pressure insertion and antibiotic inclusions upon the mechanical properties of polymethylmethacrylate. Clin Orthop 1976; (121): 67-73.

Wroblewski B M, Siney P D, Fleming P A. Charnley low-frictional torque arthroplasty: follow-up for 30 to 40 years. J Bone Joint Surg (Br) 2009; 91 (4): 447-50.

J Orthop Sci (2011) 16:26–37
DOI 10.1007/s00776-010-0007-1

ORIGINAL ARTICLE

A novel technique for impaction bone grafting in acetabular reconstruction of revision total hip arthroplasty using an ex vivo compaction device

Haruhiko Akiyama · Takkan Morishima · Mitsuru Takemoto · Koji Yamamoto · Hiromi Otsuka · Toshiki Iwase · Tamon Kabata · Tsunemitsu Soeda · Keiichi Kawanabe · Keiji Sato · Takashi Nakamura

Received: 19 May 2010 / Accepted: 7 September 2010 / Published online: 22 January 2011

Abstract
Background Impaction bone grafting allows restoration of the acetabular bone stock in revision hip arthroplasty. The success of this technique depends largely on achieving adequate initial stability of the component. To obtain well-compacted, well-graded allograft aggregates, we developed an ex vivo compaction device to apply it in revision total hip arthroplasty on the acetabular side, and characterized mechanical properties and putative osteoconductivity of allograft aggregates.

Methods Morselized allograft bone chips were compacted ex vivo using the creep technique and subsequent impaction technique to form the bone aggregates. Impaction allograft reconstruction of the acetabulum using an ex vivo compaction device was performed on eight hips. The mechanical properties and three-dimensional micro-CT-based structural characteristics of the bone aggregates were investigated.

Results In clinical practice, this technique offered good reproducibility in reconstructing the cavity and the segmental defects of the acetabulum, with no migration and no loosening of the component. In vitro analysis showed that the aggregates generated from 25 g fresh-frozen bone chips gained compression stiffness of 13.5–15.4 MPa under uniaxial consolidation strain. The recoil of the aggregates after compaction was 2.6–3.9%. The compression stiffness and the recoil did not differ significantly from those measured using a variety of proportions of large- and small-sized bone chips. Micro-CT-based structural analysis revealed average pore sizes of 268–299 μm and average throat diameter of pores in the bone aggregates of more than 100 μm. These sizes are desirable for osteoconduction, although large interconnected pores of more than 500 μm were detectable in association with the proportion of large-sized bone chips. Cement penetration into the aggregates was related to the proportion of large-sized bone chips.

Conclusion This study introduces the value of an ex vivo compaction device in bone graft compaction in clinical applications. In vitro analysis provided evidence that compaction of sequential layers of well-compacted, well-graded bone aggregates, i.e., the aggregates comprising smaller sized chips at the host bone side and larger sized chips at the component side, may have the advantages of initial stability of the acetabular component and biological response of the grafted aggregates.

H. Akiyama (✉) · M. Takemoto · K. Yamamoto · T. Soeda · T. Nakamura
Department of Orthopaedics, Kyoto University,
54 Shogoin-Kawahara cho, Sakyo, Kyoto 606-8507, Japan
e-mail: hakiyama@kuhp.kyoto-u.ac.jp

T. Morishima · H. Otsuka · K. Sato
Department of Orthopaedics, Aichi Medical University,
Nagakute, Aichi 480-1195, Japan

T. Iwase
Department of Orthopaedics, Hamamatsu Medical Center,
328 Tomitsuka-cho, Naka-ku, Hamamatsu,
Shizuoka 432-8580, Japan

T. Kabata
Department of Orthopaedics, Kanazawa University,
13-1 Takaramachi, Kanazawa, Ishikawa 920-0934, Japan

K. Kawanabe
Department of Orthopaedics, Kobe City Medical Center General Hospital, 4-6, Minatojimanakamachi, Chuo-ku, Kobe,
Hyogo 650-0046, Japan

Introduction

Total hip arthroplasty (THA) is one of the most successful procedures used to treat various hip disorders. Recent trends in a longer life expectancy of the population and an increased prevalence of THA in younger patients have led to an increase of the number of revision THAs. A major problem in a revision of a failed acetabular component is the loss of bone stock, which impairs implantation of new prosthetic components. The principles of acetabular reconstruction in revision THA are to restore pelvic bone stock, to create an acetabular bone bed for achieving stable fixation of the implants, and to rebuild an anatomical hip center with acceptable hip biomechanics and thereby to optimize joint stability.

Impaction bone grafting with morselized bone grafts is an attractive technique for restoring bone stock in acetabular reconstruction [1, 2]. This is a technically demanding option, and a wide variation in long-term outcomes has been reported [3–6]. Morselized bone chips are impacted layer by layer into the contained defects of the acetabulum with progressive forceful compaction in vivo using a metal impactor and slap hammer. This creates a neoacetabulum of an adequate new implant bed into which the acetabular component is implanted. The initial stability of the implant is essential for long-term survival, and it is likely that the initial stability of the acetabular component is determined mostly by compression resistance and interparticle shear resistance of the grafted layer, which can be affected by many parameters, including the initial stiffness and the size and quality of the bone chips [7–11]. In the standard technique of impaction bone grafting, the bone chips are impacted vigorously by a slap hammer to gain adequate stiffness of the graft aggregates, but intraoperative fractures of a thin-walled acetabular cortex are often encountered [6, 12]. Because there is no specific indicator for the intraoperative determination of when the graft has been compacted adequately, the surgeon may perform the procedure with undercompaction of the graft, resulting in instability and subsequent subsidence of the implant.

To avoid variability in clinical outcomes between surgeons, we developed a new technique of impaction bone grafting using an ex vivo compaction device. In this technique, sterilized washed morselized allograft bone chips are compacted ex vivo using the creep technique and the impaction technique to form various shapes of well-compacted, well-graded bone aggregates, which are then impacted into the contained cavity in vivo using the creep technique with impactors. In clinical practice, this technique offers good reproducibility when reconstructing the cavity and the segmental defects of the acetabulum. In this study, we introduce this new technique, and we describe the mechanical properties and three-dimensional (3D) micro-CT-based structural characteristics of the bone aggregates generated by this method to determine proper mechanical properties, osteoconductivity, and cement penetration of the bone aggregates for impaction bone grafting with morselized bone chips.

Materials and methods

Bone material

A whole femoral head was procured from a living donor at the time of primary THA for osteoarthritis. Donor selection, bone sterilization, and preservation were performed under the guidelines issued by the Japanese Society of Orthopedic Surgery. After removal of remnants of articular cartilage and synovial lining, donated bones are quarantined at −80°C for 6 months.

Graft preparation

Deep-frozen bone was sterilized by pasteurization using Lobator sd-2 (Telos, Marburg, Germany), and then ground into morselized bone chips in a bone mill (Japan Medical Materials, Osaka, Japan) once or twice to produce large- or small-sized particles, respectively (Fig. 1a). The size of the morselized particles was measured as described previously [13]: Large- and small-sized chips were 10.9 ± 1.9 and 3.69 ± 0.24 mm, respectively. Bone chips were placed into a sieve and washed using high-speed pulsatile lavage with normal saline solution to remove fat, marrow, and blood clots.

The ex vivo compaction device

The ex vivo compaction device was made of titanium alloy and stainless steel (Fig. 1b–d). This device was leverage equipped with a 50.6 cm lever. The stainless steel cylinder had an inner diameter of 46 mm, a height of 50 mm, and a wall thickness of 5.9 mm. The narrow gap (0.1 mm) between the base of the device and the cylindrical chamber allowed for fluid exudation. The inner molds were placed in the cylinder, the piston was placed on top, and compression force was then loaded with a stainless lever (Fig. 1d). Several shapes of the inner molds were provided to make a variety of shapes of the bone aggregates, including disc and lens shapes for medial wall defects of the acetabulum and thick talon shape for the peripheral wall defects (Fig. 1i).

Operating procedures

Impaction allograft reconstruction of the acetabulum using the ex vivo compaction device was performed on eight hips

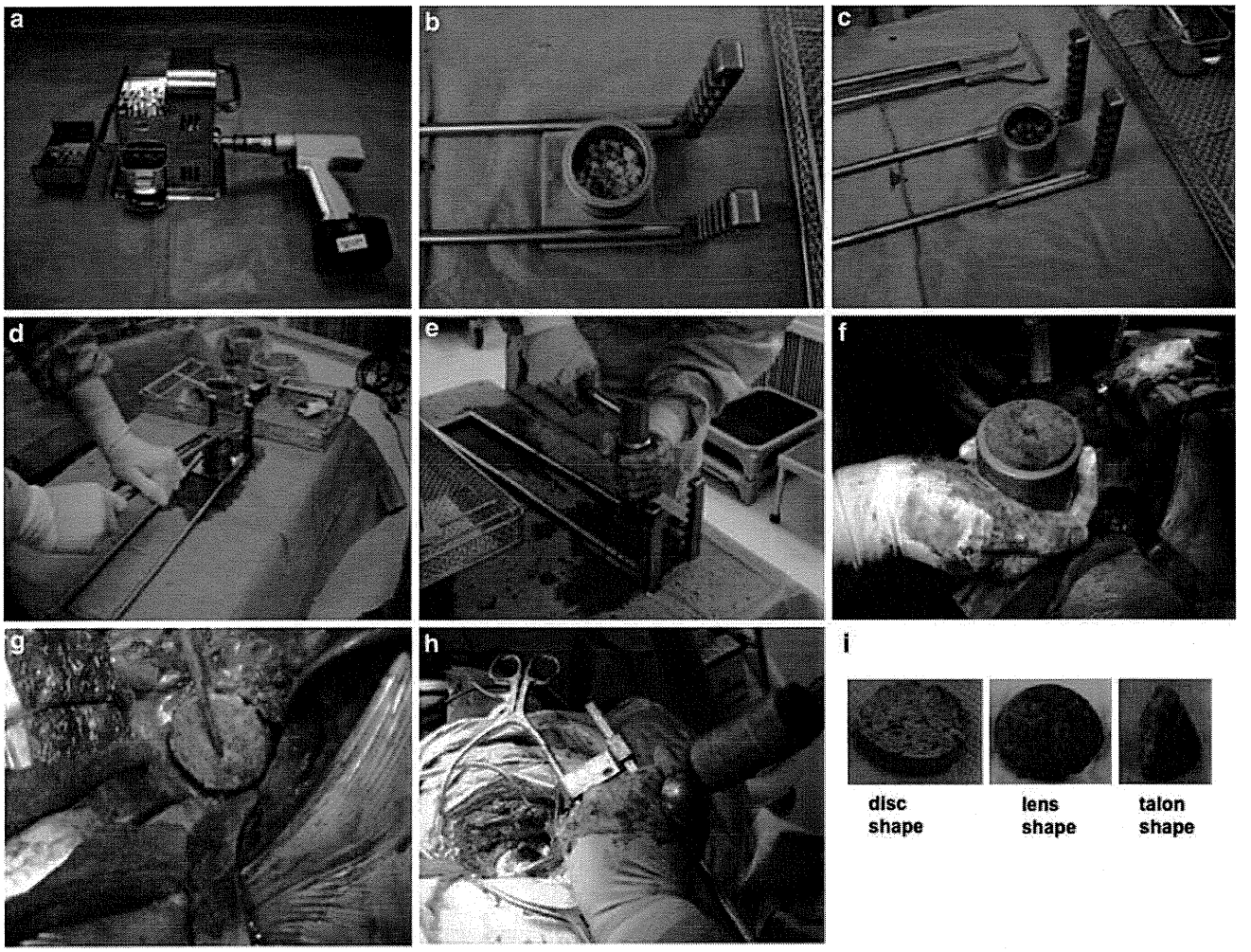

Fig. 1 Operating procedures of impaction bone grafting using the ex vivo compaction device in the acetabular reconstruction. **a** The bone mill used in this study. **b** Sterilized washed morselized allograft bone chips are placed in the chamber. **c** The patient's fresh blood is added. **d** Compression force is applied using the creep technique. **e** Impaction force is applied by the metal slap hammer. **f** The well-compacted, well-graded bone aggregate is formed. **g** The bone aggregate is grafted into the acetabulum. **h** The creep consolidation and additional light or moderate impaction form a good compacted layer within the acetabular defect. **i** Various shapes of bone aggregates can be produced

in eight patients (Table 1). All patients were female, and their average age was 63.5 years (range 48–74 years). The reasons for primary revision were aseptic loosening of the acetabular socket in five hips, migration of the bipolar outer head in two hips, and migration of the vitallium cup in one hip. Acetabular deficiencies were classified using the American Academy of Orthopaedic Surgeons (AAOS) classification [14]: type 2 in two hips and type 3 in six hips. Operations were performed through an anterolateral or posterolateral approach. After removal of the acetabular component, cement, and granulation tissues, the acetabular bone defect was assessed. The acetabular host bone was reamed until a bleeding bone bed was created or small drill holes were made for revascularization of the host bone. If necessary, segmental wall defects were contained with X-change metal mesh (Stryker Benoist Girard, Herouville-Saint-Clair, France) for peripheral wall defects and/or medial wall defects. To produce densely compacted bone aggregates for impaction bone grafting in acetabular reconstruction by an ex vivo compaction device, an adequate amount of bone chips was placed into the cylinder of the ex vivo compaction device, and 5 ml of fresh patient blood was fed into the stainless steel cylindrical chamber (Fig. 1b, c). Compaction was performed using the creep technique with a lever producing a constant compaction force for 90 s, and then a heavy impaction force was delivered five times with a metal slap hammer [15] (Fig. 1d, e). The compaction force reached a maximum of 3,300 N in the creep technique, and the heavy impaction by the hammer reached a maximum of 4,750 N (detailed data not shown). Various shapes of the bone aggregates were generated: lens or disc shaped for medial wall defects and

Table 1 Clinical cases

Case	Gender	Age (years)	AAOS classification	Cause of revision	Merle d'Aubigné and Postel score (pre-operation)	Merle d'Aubigné and Postel score (post-operation)	Follow-up period (months)
1	F	62	Type 3	Socket loosening	7	16	16
2	F	74	Type 3	Socket loosening	10	14	11
3	F	70	Type 3	Socket loosening	13	14	9
4	F	58	Type 3	Socket loosening	8	18	13
5	F	67	Type 2	Migration of bipolar outer head	10	16	13
6	F	65	Type 2	Migration of bipolar outer head	15	15	10
7	F	48	Type 3	Migration of vitallium cup	10	15	16
8	F	64	Type 3	Socket loosening	8	17	12

thick talon shaped for segmental defects under a metal mesh (Fig. 1i). The bone aggregates generated seemed dry and had enough stiffness to be held by a forceps (Fig. 1f, g). The bone aggregate was placed into the contained cavity with a constant compression force delivered using an impactor, and light or moderate impaction with a nylon hammer or a mallet (Fig. 1g, h). An X-Change metal mesh or an acetabular reconstruction plate (KT plate, Japan Medical Materials, Osaka, Japan) was used in all hips: a metal mesh for a segmental defect in three hips, for a medial wall defect in one hip, and a KT-plate in four hips in which a well-contained cavity was not obtained. A cross-linked ultra-high-molecular-weight polyethylene cup was cemented into the newly formed acetabular cavity. Before this operation, we obtained informed consent from the patients and their families.

Assessment of mechanical properties

The disc-shaped bone aggregates were produced by an ex vivo compaction device with 25 g of the indicated proportion of the mixture of large- and small-sized morselized bone chips: 25 g of large-sized bone chips in group 1, 16.7 g of large-sized and 8.3 g of small-sized bone chips in group 2, 8.3 g of large-sized and 16.7 g of small-sized bone chips in group 3, and 25 g of small-sized bone chips in group 4 ($n = 3$ for each group). The bone density of the bone aggregates comprising various sizes of 25 g of morselized bone chips was measured. Compression stiffness was measured by loading the bone aggregates in a uniaxial load-testing machine (Model 1123, Instron, Norwood, MA). The crosshead speed was 1 mm/min. The bone aggregates were compressed until 3,000 N without intervening stress relaxation. The load of 3,000 N is equivalent to the load applied to the hip joint when a person weighing 70 kg stands on one leg. The compression stiffness was calculated by the slope of the linear region in the compression stress–strain curve. The recoil was determined using the creep recovery of bone aggregates after unloading the compaction force, which represents a deformation rate relative to the initial thickness measured 90 s after ex vivo compaction.

Micro-CT-based structural analysis

Micro-CT-based structural analysis was performed based on our previous studies of porous biomaterials [16], and some modified algorithms were developed for this study. The void (pore) structure of the bone aggregates was assessed using a micro-CT system (SMX-100 CT SV3, Shimazu, Kyoto, Japan). The specimen in a cylinder made of acrylic resin was mounted on a rotatory stage and scanned in its entirety. Reconstructed images comprised 512 × 512 × 431 voxels, with a voxel size of 20 μm. These images were processed with a combination of free-ware (Image J, NIH, USA, http://rsb.info.nih.gov/ij/) and commercially available software (VG Studio MAX 2.0, Volume Graphics, Germany). The sequential analysis was conducted as follows. The image stacks were first read in as 3D slice series and subjected to image enhancement optimization by adjusting image contrast, brightness, and gamma value to highlight the contrast between the void area and the bone aggregates. Images were then smooth filtered (e.g., Gaussian filter) to reduce noise. The smoothed images then underwent a segmentation process using a 3D adaptive thresholding plugin for Image J (Adaptive 3D Threshold, C. Henden and J. Bache-Wiig, http://www.pvv.org/~perchrh/imagej/). This segmentation process converted each image to a binary image where the pixel population is assigned to either the foreground (bone) or the background (void).

For two-dimensional (2D) analysis, the binarized image stacks were subjected to 2D image processing to determine average pore size and pore size distribution. Using the watershed process in Image J, pores adjacent to each other were separated automatically, and pore area and perimeter

were measured quantitatively. The 2D pore size was calculated using the following equation:

$$PS_{2D} = \frac{4 \times PA}{PP},$$

where PS_{2D} is the 2D pore size, PA is the pore area, and PP is the pore perimeter. All pores in the image stacks were measured, and the pore size distributions were represented by a line histogram.

Image J and VG Studio MAX were used for 3D geometrical analysis. First, the binarized 3D image stacks were subjected to the Local Thickness plugin for Image J (RP. Dougherty and K–H. Kunzelmann, http://www.optinav.com/imagej.html). This plugin computed the local thickness of the 3D image stacks, defined as the diameter of the largest sphere that fits inside the pore and contains the point. The number of voxels with respective local thickness values was taken as the volume of pores with the corresponding diameter. Interconnected pores were defined as the pores that connected to the outer surface, and they were detected easily by tracing the interconnections. For the interconnectivity analysis, voxels with local thickness less than the respective values were set to foreground (blocking pore throats) [16]. The interconnected pore volume was then measured and regarded as the volume of the pore with a corresponding pore throat size. Cumulative volume fraction distribution was computed and then differentiated to give the pore size and pore throat size distributions.

Cement penetration

Ten grams of Simplex P bone cement (Stryker, Kalamazoo, MI, USA) with 0.25 ml of Indian black ink was prepared using a vacuum cement mixing system and applied to a bone aggregate in an acryl cylinder using an acetabular pressurizer (DePuy Orthopaedics, Inc., Warsaw, IN). After all the bone chips were removed, the maximal depth of cement penetration into the bone aggregates was measured ($n = 3$ for each group).

Statistical methods

In the compression test and the evaluation of cement penetration, three specimens were prepared for each composite condition of the bone aggregates, as shown in Figs. 3 and 5. The data in this study were analyzed using Dunnett's multiple comparison test. A p value <0.01 for the difference in values compared with those in group 1 was considered significant.

Institutional review board approval was obtained for publication of the study. The patients and their family were informed that data from the cases would be submitted for publication and gave their consent.

Results

Densely compacted bone aggregates were achieved in the acetabular reconstruction

The follow-up period of eight hips with impaction allograft reconstruction of the acetabulum using the ex vivo compaction device averaged 12.5 ± 2.6 months (range 9–16 months) (Table 1). The preoperative Merle d'Aubigné and Postel Score [17] of 10.1 ± 2.7 points improved to 15.6 ± 1.4 points postoperatively. No intraoperative complications occurred in any patient. Postoperative radiograms and CT showed densely packed allografts in the acetabular defect (Fig. 2). Neither migration nor loosening of the component was detected, indicating that initial stability of the component was sufficient in this procedure.

Compression stiffness of the bone aggregates did not differ significantly according to the size of bone chips

Bone density and mechanical properties of the bone aggregates made by an ex vivo compaction device were analyzed by in vitro experiments. First, the bone density of the bone aggregates comprising various sizes of 25 g of morselized bone chips was measured (Table 2). The bone density of each bone aggregate comprising various proportions of large- and small-sized bone chips ranged from 1.34 to 1.50 g/cm^3 and did not differ significantly between groups, although there was a slight correlation between the apparent density and size of the morselized bone chips. Next, the compression stiffness was measured by loading the bone aggregates in a uniaxial load-testing machine (Fig. 3a). The regression plot of stiffness versus strain showed that the mean final modulus of the bone aggregates was 13.5–15.4 MPa (Fig. 3b, c). The compression stiffness did not differ significantly between bone aggregates comprising only large-sized bone chips and those comprising small-sized bone chips, although there was slight correlation between compression stiffness and size of the morselized bone chips (Fig. 3c). The recoil was calculated in relation to the proportion of the large- and small-sized bone chips after the impaction force on the bone aggregate was released in the ex vivo compaction device. Interestingly, recoil occurred at 2.6–3.9% of the initial height of the aggregates, but did not differ significantly between the

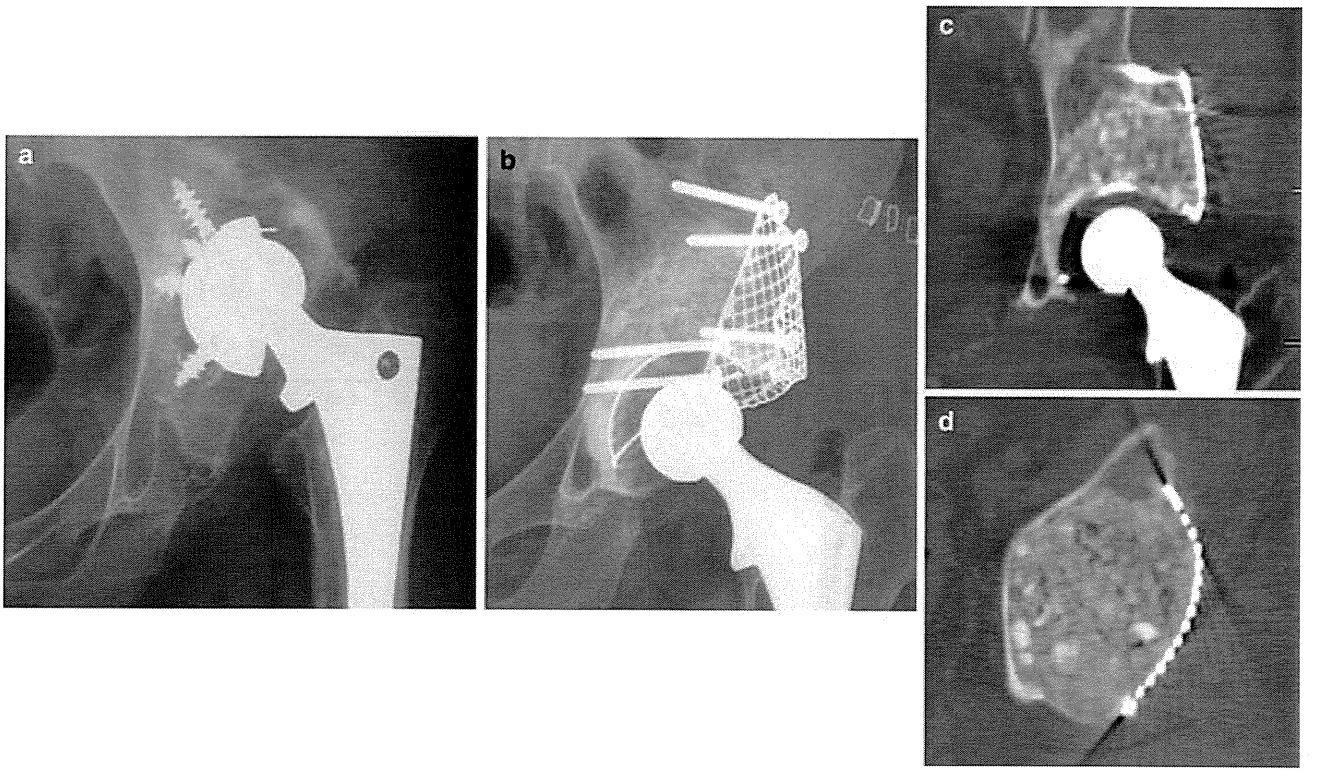

Fig. 2 Radiographs and CT images of the clinical cases. **a** Loosening of the acetabular component was revised using the impaction bone grafting technique. A postoperative radiograph **b** and CT images (**c**, **d**) show well-compacted bone grafting in an AAOS type 3 acetabular defect

Table 2 Bone density of the aggregates

Group	Ratio large size:small size	Mean ± SD (g/cm^3)	*p* value
1	All large-sized chips	1.34 ± 0.11	
2	2:1	1.48 ± 0.04	0.168
3	1:2	1.39 ± 0.03	0.677
4	All small-sized chips	1.50 ± 0.09	0.068

aggregates of different bone chip sizes (Fig. 3d). These results indicate that the ex vivo compaction device can produce well-compacted, well-graded bone aggregates with adequate mechanical stiffness from various sizes of the morselized bone chips.

The bone aggregates have a proper porous structure for osteoconduction

Two-dimensional pore size

Images of the microstructures of the bone aggregates obtained with micro-CT showed the composition of various sizes of morselized bone chips with a relatively heterogeneous distribution of pore sizes (Fig. 4a). The pore sizes of the bone aggregates were quantified from the image stacks, and the 2D pore size distributions are shown in Fig. 4b. The average pore size in the bone aggregates was 268–299 μm (Table 3), which is reported as the proper size for bone growth [18, 19].

Three-dimensional pore size

Further analysis of the void structure of the bone aggregates was performed three dimensionally (Fig. 4c, d), and it revealed that more than 95% of the pores in the bone aggregates possessed a throat diameter greater than 100 μm (Table 3), which is reported as desirable for tissue differentiation and osteoconduction [16]. Large pores with a diameter of more than 500 μm, which may be too large for bone growth [18, 19], tended to increase with the proportion of large-sized chips (Table 3). The mean porosity, pore size, pore throat size, volume fraction of pores with a narrow throat (less than 100 μm), and fraction of pores with a large diameter (more than 500 μm) were quantified from the micro-CT images and are shown in Table 3.

Bone aggregates made by large-sized bone chips exhibited better cement penetration

Cement penetration affects shear strength of the bone aggregates and the initial stability of the acetabular

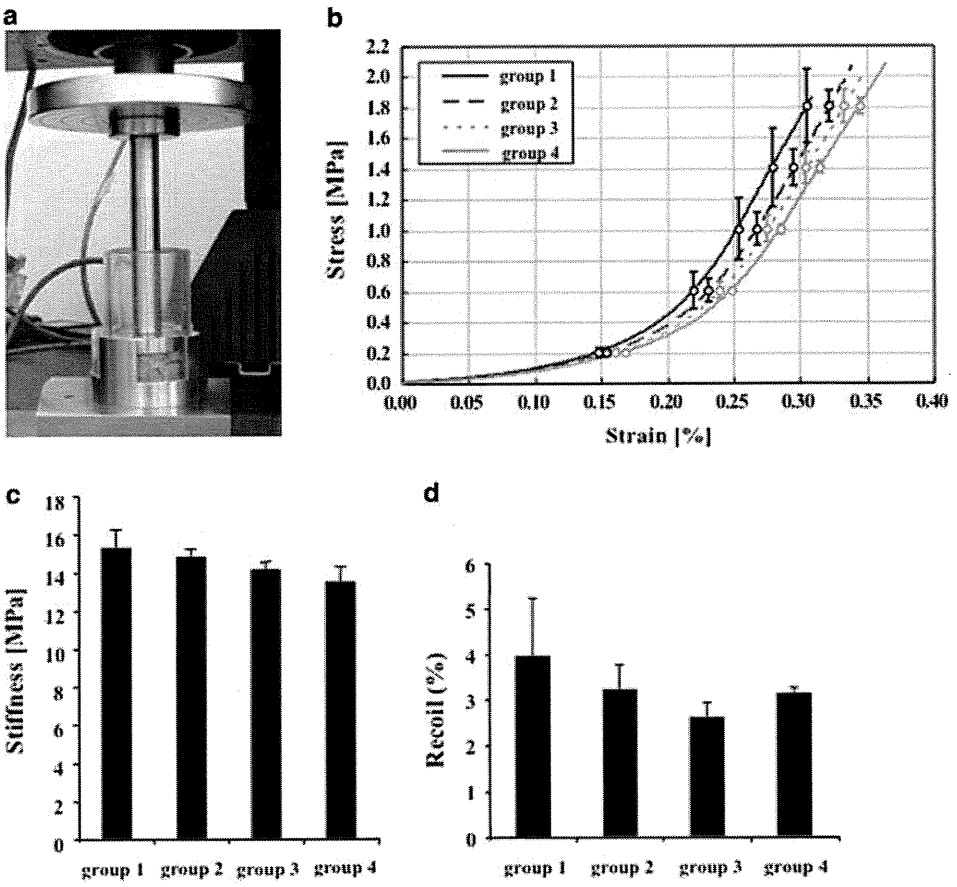

Fig. 3 Measurement of compression stiffness and recoil of the bone aggregates. **a** The force is measured with a load cell during constant displacement of the impactor gliding inside the cylinder containing the bone aggregate. **b** Compression stress versus strain curve for each specimen. **c** Compression stiffness is slightly but nonsignificantly higher in the bone aggregate containing only large-sized chips than in that containing small-sized chips. **d** Recoil of the bone aggregates does not differ significantly between the specimens

component [20]. The maximal depth of cement penetration depended on the size of the grafted bone chips (Fig. 5a, b). The average cement penetration depths were 0.76 ± 0.023 cm for the bone aggregates comprising only large-sized bone chips and 0.32 ± 0.056 cm for those comprising only small-sized bone chips.

Discussion

Impaction bone grafting in revision THA offers creation of a stable acetabular bone bed, secure prosthetic fixation, and restoration of bone stock. To gain successful clinical outcomes, bone graft preparation with morselized bone chips of various sizes is important for initial stability of the acetabular component and biological fixation of the component to the underlying host bone. However, this procedure is still technique-dependent, and there are no specific guidelines on how to produce well-compacted, well-graded bone aggregates having good mechanical and biological characteristics with various sized bone chips.

Mechanical properties of the bone aggregates

The initial stability of the acetabular component depends largely on the stiffness of the morselized allografts, which is related to the compression strength and the shear strength of the bone aggregates [7, 8, 11, 21, 22]. The principal concept of impaction bone grafting has been analyzed extensively, and it is likely that the mechanical characteristics of the bone aggregates obey the soil mechanics theory [23]. According to the Mohr-Coulomb failure criterion, the shear strength depends on the compression stress produced by the load, the angle of shearing resistance, and the interlocking of the bone particles. Thus, the impaction force has a substantial effect on the compression stiffness and shear strength of the graft aggregates. Morselized bone chips exhibit viscoelastic and viscoplastic behavior with partly recoverable and partly unrecoverable deformity under load [15]. Increasing the stiffness of the graft aggregates requires a maximal impaction force, which crushes the bone particles. However, administration of intermittent hard blows by a metal slap hammer in vivo dramatically increases the fracture risk of a thin medial

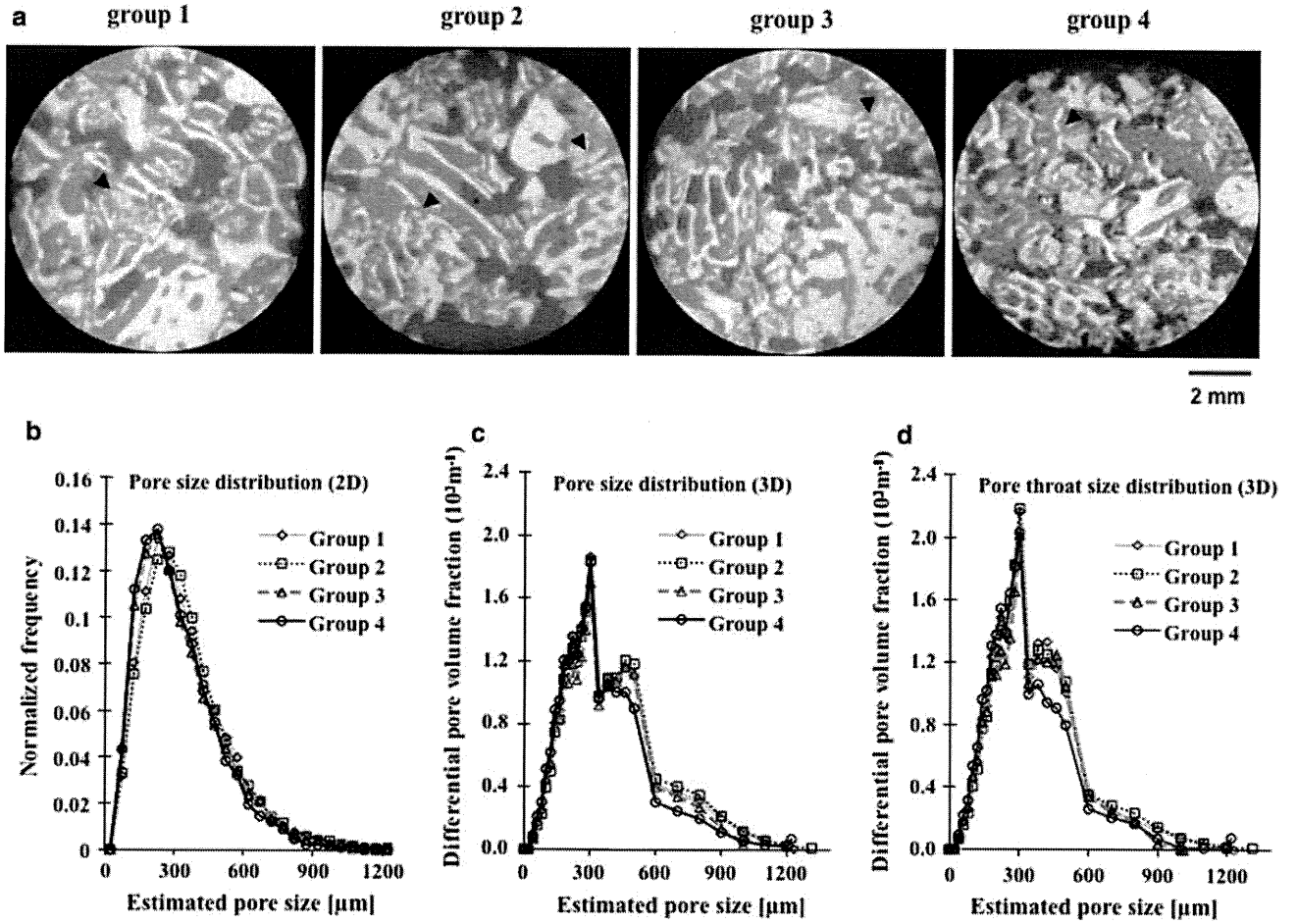

Fig. 4 Micro-CT-based structural analysis. **a** Micro-CT image of each specimen. *Arrowheads* denote crushed trabeculae. **b–d** Distribution of pore size based on **b** 2D analysis, **c** 3D analysis, and **d** pore throat size in each sample

Table 3 2D and 3D structural analysis of bone aggregates

Group	2D analysis	3D analysis				
	Pore size	Porosity (%)	Pore size[a]	Pore throat size[a]	Pore with narrow throat[b] (%)	Large pore[c] (%)
1	299 ± 191	63.1	393 ± 210	361 ± 186	2.7	26.4
2	299 ± 188	63.6	405 ± 211	372 ± 192	2.6	28.9
3	278 ± 183	57.4	376 ± 183	339 ± 146	3.4	23.8
4	268 ± 177	56.4	354 ± 191	328 ± 168	4.0	19.1

[a] Mean ± SD (μm)

[b] Volume fraction of pore with narrow throat (diameter less than 100 μm) in total pore

[c] Volume fraction of large pore (diameter more than 500 μm) in total pore

acetabular wall, and therefore a graft compaction method is required to yield greater strength and stiffness of the bone aggregates with increasing compaction force but with less risk of fracture. Albert et al. [15] reported that the creep technique, which involves holding a constant compaction force of 300 N for 90 s, improved the stiffness and shear strength by 14 and 16%, respectively, in vitro and suggested that the creep technique could provide a lower risk of intraoperative fracture over the use of larger impaction forces. However, they also showed that the higher impaction force increased stiffness and shear strength by 93 and 164%, respectively. On the basis of their data, a combination of the creep technique and the higher impaction force produced with a metal slap hammer may

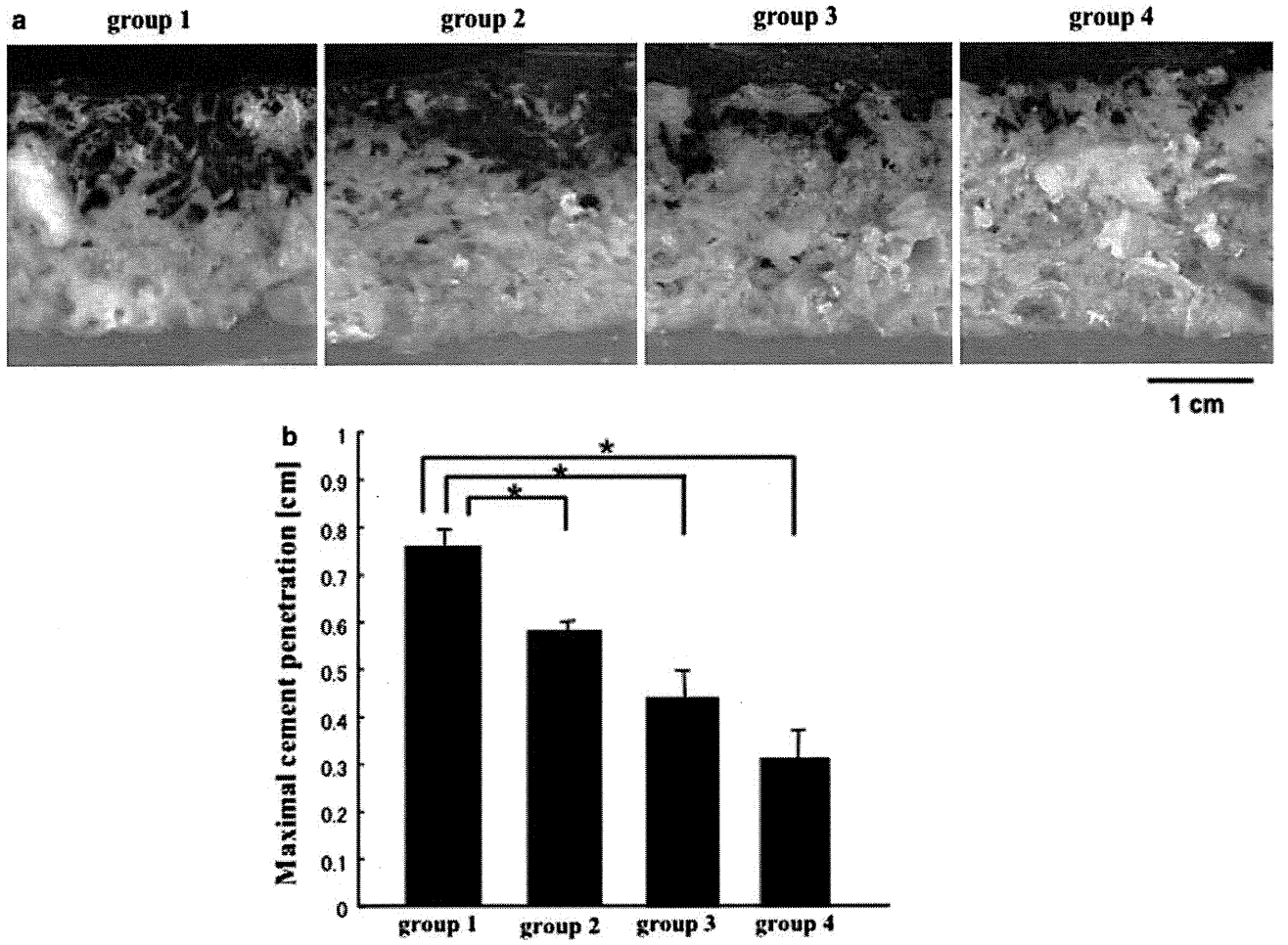

Fig. 5 Cement penetration into the bone aggregates. **a** Bone cement containing Indian black ink is applied to the bone aggregates with an acetabular pressurizer. **b** Maximal depth of cement penetration is increased in proportion to the amount of large-sized chips. *Asterisk* denotes significant difference $p < 0.01$

markedly improve the compression stiffness and shear strength of the bone aggregates. The ex vivo compaction device used in our study can hold a constant compaction force of more than 3,000 N and heavy load impaction force of more than 4,700 N. The compression stiffness of our postimpaction bone aggregates was 13.5–15.4 MPa, which is similar to the value reported in other studies [9, 24] and to that of cancellous bone from the femoral head as previously reported [25].

Bone density

The mechanical property of the bone aggregates also depends on the density of the packed bone chips and greater interparticulate surface area contact; increasing these variables produces more stiffness and less recoil of the bone aggregates [7, 11, 21]. To reduce the void space and to increase the interdigitation between bone particles, we removed fat, bone marrow, and blood clots by washing the morselized bone chips using high-speed pulsatile lavage. The patient's fresh blood was added to the sterilized washed morselized bone chips in the ex vivo compaction device because a small amount of fibrin formation decreases the recoil and increases the shear strength of the bone aggregates [26]. Importantly, slow compaction by the creep technique using the ex vivo compaction device allowed sufficient time for excess fluid exudation and deformation of the bone particles, and therefore produced dense and stiffer aggregates. The graft density of our bone aggregates was 1.34–1.50 g/cm^3, which is greater than that reported previously [27].

Size of the bone chips

The size of the bone chips also affects the stiffness of the bone aggregates. Bolder et al. [28] recommended larger sized chips for the acetabulum. They produced large bone chips (8–10 mm in diameter) by hand using a rongeur and